AGU PUBLICATIONS

JGR

Journal of Geophysical Research: Space Physics

RESEARCH ARTICLE
10.1002/2015JA021319

Key Points:
- Presence of field-aligned potentials does not hugely alter thermospheric flows
- Variations in Pedersen conductance have strongest effects on system
- Field-aligned potentials strongly affect predicted auroral brightnesses

Correspondence to:
L. C. Ray,
licia.ray@ucl.ac.uk

Citation:
Ray, L. C., N. A. Achilleos, and J. N. Yates (2015), The effect of including field-aligned potentials in the coupling between Jupiter's thermosphere, ionosphere, and magnetosphere, *J. Geophys. Res. Space Physics*, *120*, 6987–7005, doi:10.1002/2015JA021319.

Received 10 APR 2015
Accepted 17 JUL 2015
Accepted article online 24 JUL 2015
Published online 19 AUG 2015

©2015. The Authors.
This is an open access article under the terms of the Creative Commons Attribution License, which permits use, distribution and reproduction in any medium, provided the original work is properly cited.

The effect of including field-aligned potentials in the coupling between Jupiter's thermosphere, ionosphere, and magnetosphere

L. C. Ray[1,2,3], N. A. Achilleos[1,3], and J. N. Yates[2]

[1]Department of Physics and Astronomy, University College London, London, UK, [2]Space and Atmospheres Group, Imperial College London, London, UK, [3]Centre for Planetary Sciences, University College London, London, UK

Abstract Jupiter's magnetosphere-ionosphere-thermosphere system drives the brightest, steadiest aurora in our solar system. This emission is the result of an electrical current system, which couples the magnetosphere to the planetary atmosphere in an attempt to enforce the corotation of the middle magnetospheric plasma. Field-aligned currents transfer angular momentum from the atmosphere to the magnetosphere. In the equatorial plane, the field-aligned currents diverge into radially outward currents, which exert a torque on the plasma due to the $\mathbf{J} \times \mathbf{B}$ forces. Equatorward ionospheric currents exert an opposite torque on the ionosphere, which interacts with the thermosphere via ion-neutral collisions. The upward field-aligned currents result in auroral electron precipitation, depositing energy into the high-latitude atmosphere. This energy input is a possible candidate for explaining the large thermospheric temperature measured by the Galileo probe at equatorial latitudes; however, previous atmospheric circulation models have shown that the bulk of the energy is transported poleward, rather than equatorward. We present numerical results of Jupiter's coupled magnetosphere-ionosphere-thermosphere system including, for the first time, field-aligned potentials. The model is compared with three previously published works. We find that the rotational decoupling of the magnetospheric and thermospheric angular velocities in the presence of field-aligned potentials tempers the thermospheric response to the outward transport of magnetospheric plasma, but this is a secondary effect to variations in the Pedersen conductance.

1. Introduction

Jupiter's thermosphere, ionosphere, and magnetosphere form a complex coupled system wherein angular momentum and energy are exchanged between the three regions. Ion-neutral collisions couple the colocated thermosphere and ionosphere, while electrical currents and the planetary magnetic field connect the ionosphere and magnetosphere. Understanding this dynamic system is one of the keys to explaining the high thermospheric temperatures measured by the Galileo probe, which penetrated Jupiter's atmosphere in the equatorial region. At the exobase, the measured temperature was ~900 K, with the temperature profile decreasing to ~200 K at the bottom of the thermosphere [*Seiff et al.*, 1998].

At equatorial latitudes, the obvious candidate to explain the high temperatures is solar heating; however, *Strobel and Smith* [1973] showed that solar EUV heating alone could only produce a maximum vertical difference of ~60 K between the top and bottom of the thermosphere. Therefore, an "energy crisis" exists at Jupiter, with the outstanding question being: how does the thermosphere get heated to such high temperatures? Possible mechanisms include the following: upward propagating gravity and acoustic waves [*Young et al.*, 1997; *Matcheva and Strobel*, 1999; *Hickey et al.*, 2000; *Schubert et al.*, 2003]; energetic particle precipitation [*Grodent et al.*, 2001]; Joule heating, with and without fluctuating electric fields [*Smith et al.*, 2005; *Smith and Aylward*, 2009]; the redistribution of deposited auroral energy by neutral winds [*Millward et al.*, 2005]; and the "pumping" of the atmosphere by compressions in the solar wind [*Yates et al.*, 2012, 2014]. This analysis explores how the presence of high-latitude field-aligned potentials affects the deposition of auroral energy at the planetary atmosphere, and the subsequent thermospheric temperature and flow profiles.

Jupiter's main auroral emission is a persistent phenomenon caused by the electron precipitation associated with the upward portion of the magnetosphere-ionosphere current system that enforces the corotation of the

magnetospheric plasma. The main emission has been observed at X-ray [e.g., *Branduardi-Raymont et al.*, 2008], ultraviolet (UV) [e.g., *Clarke et al.*, 1998; *Grodent et al.*, 2003; *Nichols et al.*, 2009; *Gérard et al.*, 2013], infrared (IR) [e.g., *Stallard et al.*, 2001; *Melin et al.*, 2006], and visible wavelengths [e.g., *Vasavada et al.*, 1999], with a variety of in situ and remote instruments. The location of the emission is fixed in System III, Jupiter's longitude system, such that it rotates in and out of view as seen by an Earth-based observer because the planet's magnetic axis is tilted and offset relative to its spin axis. Temporal variations in both the intensity and the location of the emission are best observed in UV wavelengths, owing to the "instantaneous" nature of the H_2 emission, the absorption of background UV sunlight by hydrocarbon haze, and the shorter integration times required to obtain a high-quality image. Using Hubble Space Telescope-Space Telescope Imaging Spectrograph spectral observations, *Gustin et al.* [2004] found that the main auroral emission was associated with precipitating energy fluxes of 2–30 mW m^{-2} and precipitating electron energies of 30–200 keV. Typically, a narrow emission, spanning ~1° at the planet [*Clarke et al.*, 2004], the auroral emission shifts as much as 3° in latitude with variations in the magnetospheric conditions, possibly related to volcanic output from Io and/or solar wind activity [*Grodent et al.*, 2003, 2008; *Nichols*, 2011; *Bonfond et al.*, 2012].

While the characteristics of the auroral electron population, acceleration region, and magnetospheric dynamics driving the aurora can be inferred from the UV emission, observations at IR wavelengths offer critical insight into the Jovian ionosphere and thermosphere, regions that are otherwise probed predominantly by solar and stellar occultations in the radio and UV wavebands. The thermospheric temperature can be estimated under the assumption of local thermodynamic equilibrium (LTE) by comparing H_3^+ emission from different transition lines. *Stallard et al.* [2002] used this method to confirm that large thermospheric temperatures also exist in high-latitude auroral regions, ranging from ~900 to 1250 K. *Melin et al.* [2006] revised the temperatures found by *Stallard et al.* [2002] to account for the non-LTE nature of the auroral atmosphere. They found that the temperature derived under the LTE assumption underestimated the actual temperature by as much as ~150 K or ~10% at altitudes above 200 km [*Melin et al.*, 2006, Figure 3]. It is also possible to determine the line-of-sight ion velocity from the H_3^+ aurora through corresponding Doppler shifts in the emission lines. *Stallard et al.* [2001] found that the location of the main auroral emission corresponds to a region of subcorotating ionospheric flows, equivalent to winds of −1.5 to −2 km s^{-1} relative to the local planetary rotation rate, with the negative sign indicating a westward velocity. These winds are the result of an anticorotational $\mathbf{J}\times\mathbf{B}$ force associated with the torque exerted on the ionosphere by the current system that transfers angular momentum to Jupiter's magnetospheric plasma and causes the main auroral emission.

Jupiter's main auroral emission is ultimately driven by the radial transport of Iogenic plasma outward through the Jovian magnetosphere. Located at ~6 R_J (Jovian radii, 1 $R_J = 7.1492 \times 10^7$ m), Io outgasses ~700–3000 kg s^{-1} of neutral material [*Delamere and Bagenal*, 2003; *Delamere et al.*, 2004]. The neutral material is ionized primarily through electron impact ionization and charge exchange processes, with effectively half lost from the magnetosphere as fast neutral species [*Delamere et al.*, 2005]. The remaining ~350–1500 kg s^{-1} of plasma must then be transported through the magnetosphere. As the plasma moves radially outward, the tendency to conserve angular momentum dictates that it rotate more slowly. However, in the collisionless MHD approximation — applicable in the Jovian magnetodisc — the plasma is frozen-in to the planetary magnetic field, which is generated by the rapidly rotating planet ($\Omega_{Jup} = 1.7735 \times 10^{-4}$ rad s^{-1}). Therefore, where the plasma deviates from rigid rotation with Jupiter, it distorts the planetary field from a poloidal configuration. Field-aligned currents develop simultaneously with this magnetic configuration and transfer angular momentum from the planetary atmosphere to the magnetospheric plasma. There are a number of physical constraints that affect the efficiency with which the planet conveys its rotation rate to the surrounding magnetospheric plasma. Working from the planet outward, these are the following: (1) the subcorotation of the thermosphere relative to the deep interior of the planet, (2) the strength and variability of the ionospheric Pedersen conductance, (3) the development of field-aligned potentials at high magnetic latitudes, and (4) the magnitude of the north-south component of the magnetic field in the center of the current sheet (under the approximation that the magnetospheric plasma can be treated as a thin disc).

The $\mathbf{J}\times\mathbf{B}$ force that accelerates magnetospheric plasma toward corotation corresponds to an anticorotational $\mathbf{J}\times\mathbf{B}$ force in the planetary ionosphere that, through ion-neutral collisions, decelerates the flow of the thermospheric neutral gas. If the collisional ion drag is persistent over many Jovian rotations or longer, it can slow the local thermosphere in the region that couples to the middle magnetosphere, provided that the transfer of angular momentum from the deep interior to the thermosphere is not efficient enough to keep the thermospheric neutrals corotational [*Huang and Hill*, 1989; *Pontius*, 1995]. *Huang and Hill* [1989] were the first to

investigate this corotation lag. Their analysis assumed that eddy diffusion was the primary transport mechanism within the Jovian atmosphere and found that the neutral atmosphere must "slip" relative to the deep interior. Such a slippage, they surmised, could be parameterized in terms of an effective ionospheric Pedersen conductance for the purposes of magnetosphere-ionosphere coupling. *Smith and Aylward* [2008] found that meridional advection, in which thermospheric gas is transported vertically upward, then poleward to higher latitudes, is a more effective means of angular momentum transport within Saturn's atmosphere, which is similar, in this context, to that of Jupiter. Their analysis used a coupled magnetosphere-ionosphere-thermosphere (M-I-T) model and suggested that a self-consistent treatment of the thermosphere is a more realistic depiction of the system rather than a uniform effective Pedersen conductance.

In the ionosphere, the peak of the Pedersen conductivity exists where the ion-neutral collision frequency is equal to the ion gyrofrequency. The ion-neutral collision frequency in Jupiter's thermosphere for H_3^+ is comparable to the gyrofrequency at pressure levels around 1 μbar. As the ion-neutral collision frequency depends on (i) the profile of the total ion density and (ii) the profile of the ion mobility, i.e., the profile of the ion drift velocity, changes in the ionospheric density will also affect the local conductivity, and hence height-integrated conductivity (hereafter called "conductance"). *Millward et al.* [2002] explored how Jupiter's ionospheric conductance changes with variations in electron precipitation energy and electron energy flux. They found that for a fixed electron precipitation energy, the conductance is directly related to changes in the electron energy flux such that increases in the incident electron energy flux enhance the conductance. However, for a constant number flux but varying electron precipitation energy, the Pedersen conductance peaked for electrons of energy ~60 keV, since electrons of greater energy precipitate into the hydrocarbon layer where recombination timescales are relatively short. *Nichols and Cowley* [2004] used the results of *Millward et al.* [2002] to derive a relationship between the Pedersen conductance and field-aligned current density. They showed that modifying the Pedersen conductance in response to auroral currents enhanced the angular momentum transfer from the atmosphere to the magnetospheric plasma.

Smith and Aylward [2009], hereafter denoted SA09, coupled an azimuthally symmetric model of Jupiter's atmosphere to the one-dimensional *Nichols and Cowley* [2004] model of magnetosphere-ionosphere currents. Their study investigated the influence of the thermosphere on the transfer of angular momentum from the planetary atmosphere to the magnetospheric plasma. They found that explicitly including the thermospheric flows on the M-I-T coupling did not significantly alter the predicted magnetospheric plasma angular velocity outside of ~30 R_J; however, the magnetospheric angular velocity inside of ~30 R_J strongly responded to the thermospheric flows. The thermosphere also responded to the M-I coupling currents, supercorotating at latitudes magnetically conjugate to the inner magnetosphere.

Yates et al. [2012], hereafter denoted Y12, extended the SA09 model to investigate M-I-T coupling current and flows appropriate for configurations of the magnetosphere related to solar wind compressions, and average conditions. They took the "average" magnetodisc size to be 65 R_J. Y12 found that the power dissipated in the atmosphere associated with the acceleration of magnetospheric plasma is increased in the expanded magnetospheric configuration relative to the compressed one. Like the *Nichols and Cowley* [2004] study, the SA09 and Y12 analyses assumed that the magnetic field lines were equipotentials (i.e., there were no electric potential drops along the magnetic field).

If the magnetospheric plasma's demand for angular momentum is such that the field-aligned currents required exceed the maximum value of the local electron thermal current density, field-aligned electric potentials will develop. In the rapidly rotating Jovian system, the cold, dense magnetospheric ions are confined to the centrifugal equator. Magnetospheric electrons are less affected by the centrifugal force and travel more readily along the field in their bounce motion. The resulting charge separation leads to an ambipolar electric field which acts to pull the ions up to higher latitudes and restrict the electrons in their planetward motion. At the ionospheric end of the flux tube, Jupiter's gravity restricts the motion of the ionospheric plasma along the magnetic field. Therefore, there is a relative lack of plasma, i.e., current carriers, at high magnetic latitudes where the magnitude of the sum of the gravitational and centrifugal potentials reaches a maximum [*Su et al.*, 2003]. It is at this location where field-aligned potentials are likely to develop, boosting the remaining electron distribution into the loss cone in order to enhance the field-aligned currents flowing between the planet and magnetosphere [*Ray et al.*, 2009]. *Ray et al.* [2010], hereafter R10, showed that self-consistently including high-latitude field-aligned potentials in the M-I coupling system leads to the following: (i) the decoupling of the rotation of the ionosphere and magnetosphere where strong latitudinal gradients in the field-aligned

potential magnitude exist and (ii) the spreading of the transfer of angular momentum over a broader radial range in the magnetosphere.

Combining the analyses of SA09 and R10, the present study explores how including the rotational decoupling produced by the presence of field-aligned potentials at high magnetic latitudes affects the thermosphere-ionosphere-magnetosphere coupling, and transport of energy within the thermosphere. The paper is presented as follows: section 2 describes the coupled thermosphere-ionosphere-magnetosphere model and relevant theory, section 3 compares our model output to three previous studies [*Smith and Aylward*, 2009; *Ray et al.*, 2010; *Yates et al.*, 2012], and section 4 discusses the main results of our work and future avenues for exploration.

2. Theoretical Background

2.1. Atmosphere Model

Jupiter's thermosphere is described using a 3-D general circulation model (GCM) with zero azimuthal gradients, also known as 2.5-D model. The GCM has a latitudinal resolution of 0.2° and a vertical resolution of 0.4 pressure scale heights. Meridional and azimuthal flows are calculated as a function of altitude and latitude with the lack of azimuthal gradients enforcing an azimuthally symmetric thermosphere. The atmosphere's evolution with time is governed by the momentum, energy, and continuity equations [*Achilleos et al.*, 1998]. At the lower boundary, the pressure and temperature are fixed at 2 μbar and 262 K, respectively. For simplicity, the planetary magnetic field at the atmosphere is assumed to be radial with a constant strength of 1.9 B_J, where $B_J = 426,400$ nT (the equatorial field strength at the planet), across all latitudes in alignment with previous studies *Nichols and Cowley* [2004]; *Smith and Aylward* [2009]; *Yates et al.* [2012] .

The model thermosphere is composed of H, H_2, and He. At the lower boundary, helium and molecular hydrogen dominate the number density, with ~90% and ~10% of the population, respectively. The density of He quickly falls off with altitude and at the upper boundary of the model, atomic H (~95%) dominates over H_2 (~5%). Density and pressure profiles are initialized using the *Grodent et al.* [2001] Jovian atmosphere corresponding to diffuse auroral precipitation. Initially, the atmosphere is cold with a uniform temperature of 262 K, equal to that at the lower boundary pressure of 2 μbar from *Grodent et al.* [2001]. Atmospheric chemistry is not included in the model. Rather, our model implements a simplified description of the ionosphere through use of the vertical Pedersen and Hall conductivity profiles. A detailed description of the initialization of the Pedersen and Hall conductivity profiles is given in Appendix B of *Smith and Aylward* [2009]. The relative variation in the altitudinal ionospheric Pedersen conductivity profile is held fixed throughout the model run as a function of pressure. The conductivity profile is then scaled according to atmospheric energy inputs to match the height-integrated Pedersen conductance calculated by the magnetospheric module described in section 2.2.1. Since the atmosphere may expand or contract with heating and cooling, expressing the relative conductivity profile as a function of pressure ensures that local maxima and minima in conductivity remain beneath a constant column mass of thermospheric gas.

The magnetospheric module treats the Jovian atmosphere as an infinitesimally thin slab; thus, it is necessary to height-average the altitudinal profile of the thermospheric angular velocity. The weighting of each vertical layer depends on the vertical profile of the ionospheric Pedersen conductivity and relative strengths of the Hall and Pedersen conductivities

$$s\omega_T = s\Omega_J + u_\phi + \left(\sigma_H/\sigma_P\right) u_\theta \tag{1}$$

where s is the distance from the spin axis, ω_T is the thermospheric angular velocity as a function of altitude, Ω_J is the Jovian angular frequency, $\sigma_{H/P}$ are the Hall/Pedersen conductivities, and $u_{\phi/\theta}$ are the azimuthal/meridional flows, calculated using the Navier-Stokes equations solved in the reference frame corotating with the planet. The effective thermospheric angular velocity, Ω_T, is a weighted mean of the local angular velocity with altitude, where the weighting is calculated using the Pedersen conductivity

$$\Sigma_P \Omega_T = \int \sigma_P \omega_T \, \mathrm{d}z \tag{2}$$

where Σ_P is the Pedersen conductance (i.e., $\Sigma_P = \int \sigma_p \, \mathrm{d}z$).

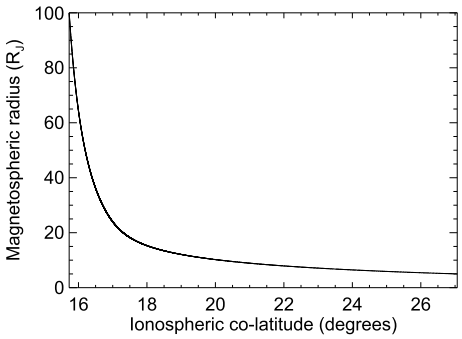

Figure 1. Relationship between the magnetospheric equatorial radius and ionospheric colatitude for the CAN-KK model.

2.2. Magnetospheric Calculation

The magnetospheric calculation is divided into four regions which are then coupled to the thermospheric module by the process described below in section 2.3. The regions are as follows: Region I, which describes the solar wind forcing on the thermosphere; Region II, which represents the boundary layer in the outer magnetosphere between the open field lines and the magnetodisc; Region III, which is the magnetodisc region that in this analysis spans from 4 R_J to 100 R_J; and Region IV, which is the inner magnetosphere. We now describe how each region is treated, starting with the magnetodisc region.

2.2.1. Magnetodisc ($4R_J < 100R_J$) (Region III)

While the ultimate source of angular momentum is Jupiter's deep interior, it is the thermosphere that communicates angular momentum to the magnetospheric plasma. We therefore adjust the torque balance equation relating the magnetosphere and ionospheric plasma to explicitly include the thermospheric angular velocity. The balance between the torques owing to the $\mathbf{J}\times\mathbf{B}$ force in the magnetospheric equatorial plane and the outward radial motion of plasma can be expressed as

$$\dot{M}\frac{\mathrm{d}}{\mathrm{d}r}\left(r^2\Omega_M\right) = 2\pi r^2 K_M B_M \tag{3}$$

where $\dot{M}$ is the radial plasma mass transport rate, r is the distance from the planet, K_M is the magnetospheric height-integrated current density, B_M is the magnitude of the north-south magnetic field in the magnetosphere, and Ω_M is the angular velocity of the magnetospheric plasma. The angular velocity of the magnetosphere can be expressed as a reference velocity with a perturbation. In this analysis, we select the reference frame of our calculations to be that of the neutral thermosphere, which is the source of angular momentum for the magnetospheric plasma, such that $\Omega_M = \Omega_T + \omega$, where Ω_T is the thermospheric angular velocity and ω is the deviation in the angular velocity of the magnetospheric plasma from corotation with the thermosphere.

The remainder of the magnetodisc calculation follows that described in detail by *Ray et al.* [2010]. In brief, the magnetospheric calculation is 1-D in the radial (or, equivalently, meridional) direction, with a fixed stepsize of $\delta r = 0.001\ R_J$. Magnetically conjugate locations in the magnetosphere and atmosphere are related via flux equivalency and map as provided in Figure 1. The radial (meridional) evolution of currents and electric fields assumes that the magnetic field lines are equipotentials until the ionospheric field-aligned current density exceeds the electron thermal current density

$$J_x = en_x\sqrt{T_x/(2\pi m_e)} \tag{4}$$

where e is the fundamental charge, m_e is the mass of the electron, and n_x and T_x are the electron number density and temperature, with the subscript x indicating that properties are evaluated at the location of minimum plasma density along the field.

When the field-aligned current density, $J^I_{||}$, is greater than J_x field-aligned potentials exist at high magnetic latitudes, boosting the electron distribution into the loss cone and increasing the field-aligned current density until either the entire electron distribution is within the loss cone, the field-aligned current density is consistent with that demanded by momentum transfer between the magnetosphere and thermosphere, or the field-aligned currents subside. The relationship between the field-aligned current density and field-aligned potential strength is [*Knight*, 1973]

$$J^I_{||} = J_x + J_x\left(R_x - 1\right)\left(1 - e^{-\left(\frac{e\Phi_{||}}{T_x(R_x-1)}\right)}\right) \tag{5}$$

where $\Phi_{||}$ is the field-aligned potential drop and $R_x = B_I/B_x$ is the magnetic mirror ratio between the top of the acceleration region (field strength B_x) and the ionosphere (field strength B_I). In a steady-state system,

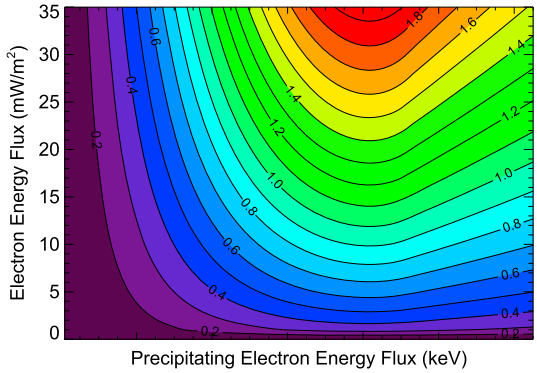

Figure 2. Variation of the Pedersen conductance with precipitating electron energy and electron energy flux from *Ray et al.* [2010] for an initial background Pedersen conductance of $\Sigma_P^{\text{Initial}} = 0.01$ mho.

changes in the magnitude of $\Phi_{||}$ with radial distance, or equivalently latitude, alter the mapping of the perpendicular electric fields through Faraday's Law. Additionally, precipitating electrons that are accelerated by the field-aligned potential modify the height-integrated Pedersen conductivity through ionization of the atmosphere, such that Σ_P is a function of both electron precipitation energy, $e\Phi_{||}$, and incident energy flux, EF, as shown in Figure 2 and described in Appendix A of *Ray et al.* [2010].

2.2.2. Poleward (Regions I and II) and Equatorward (Region IV) Flows

Poleward of the region that maps to the magnetodisc, the azimuthal flows are imposed following *Cowley et al.* [2005], similar to the analysis of Y12 and SA09 for ease of comparison. In the polar ionosphere (Region I), set here to be poleward of 10.25°colatitude, the azimuthal velocity is [*Isbell et al.*, 1984]

$$\left(\frac{\omega'}{\Omega_J}\right)_{PC} = \frac{\mu_0 \Sigma_{P_{PC}} V_{SW}}{1 + \mu_0 \Sigma_{P_{PC}} V_{SW}} \tag{6}$$

where $\left(\frac{\omega'}{\Omega_J}\right)_{PC}$ is the polar cap ionospheric angular frequency normalized to that of Jupiter, μ_0 is the permeability of free space, $\Sigma_{P_{PC}}$ is the Pedersen conductance in the polar cap, and $V_{SW} = 400$ km/s is the typical solar wind velocity. Note that the angular velocity is constant across the entire polar cap.

In the boundary layer between the polar cap and magnetodisc region, hereafter called the outer magnetosphere or Region II, the plasma flows follow the description of *Cowley et al.* [2005], with a slight modification such that the ionospheric angular velocity, $\left(\frac{\omega'(\theta_i)}{\Omega_J}\right)$, as a function of colatitude, θ_i, varies smoothly from the edge of the magnetodisc to the polar cap boundary as

$$\left(\frac{\omega'(\theta_i)}{\Omega_J}\right) = \left(\frac{\omega'}{\Omega_J}\right)_{PC} + \frac{1}{2}\left[\left(\frac{\omega'}{\Omega_J}\right)_{OM} - \left(\frac{\omega'}{\Omega_J}\right)_{PC}\right]\left[1 + \tanh\left(\frac{\theta_i - \theta_{iPC}}{\Delta\theta_{iPC}}\right)\right] + \left[\left(\frac{\omega'}{\Omega_J}\right)_{MM} - \left(\frac{\omega'}{\Omega_J}\right)_{OM}\right]\left[1 + \tanh\left(\frac{\theta_i - \theta_{iMM}}{\Delta\theta_{iMM}}\right)\right] \tag{7}$$

where θ_{iMM} is the colatitude at the boundary of the magnetodisc region, $\left(\frac{\omega'}{\Omega_J}\right)_{MM}$ is the plasma angular velocity at θ_{iMM}, and likewise the colatitude at the polar cap boundary is θ_{PC}. The magnetospheric angular velocity in the outer magnetosphere is defined as

$$\left(\frac{\omega'}{\Omega_J}\right)_{OM} = \frac{1}{2}\left(\frac{45\ R_J}{R_{MM}}\right)^2 \tag{8}$$

where R_{MM} is the radial distance at the outer edge of the magnetodisc ($R_{MM} = 100\ R_J$ in the present analysis). This equation gives values of ω'_{OM} that are higher for a more compressed magnetosphere. Finally, the width of the transition between Regions I and II is $\Delta\theta_{iPC} = 0.125°$ and

$$\Delta\theta_{iMM} = \frac{\omega'_{MM} - \omega'_{OM}}{\left.\frac{\delta\omega'}{\delta\theta}\right|_{MM}}$$

is set to ~0.5°, between Regions II and III.

Table 1. Details of the Run Parameters for Each Pair of Comparisons

	SA09	This Study	R10	This Study	Y12	This Study
Rotations Run	200	200	NA	100	50	50
Regions I & II Σ_P (mho)	0.2	0.2	0.2	0.2	0.2	0.2
Region III $\Sigma_P^{initial}$ (mho)	0.0275	0.05	0.1	0.1	0.0275	0.05
varying with	$j_{\|\|}$ [a]	($j_{\|\|}$, $j_{\|\|}\Phi_{\|\|}$)[b]	($j_{\|\|}$, $j_{\|\|}\Phi_{\|\|}$)[b]	($j_{\|\|}$, $j_{\|\|}\Phi_{\|\|}$)[b]	$j_{\|\|}$ [a]	($j_{\|\|}$, $j_{\|\|}\Phi_{\|\|}$)[b]
Region IV Σ_P (mho)	0.0275	0.05	0.1	0.1	0.0275	0.05
$\Phi_{\|\|}$ self-consistent	No	Yes	Yes	Yes	No	Yes
Ω_T feedback	Yes	Yes	No	Yes	Yes	Yes
$R_{magnetodisc}$ (R_J)	100	100	100	100	65	65
I_{outer} (MA)	100	100	86	86	100	100
$\dot{M}$ (kg s^{-1})	1000	1000	1000	1000	1000	1000

[a]The Pedersen conductance functions are based on *Nichols and Cowley* [2004].
[b]The Pedersen conductance functions are based on *Ray et al.* [2010].

For atmospheric regions that are magnetically conjugate with equatorial locations inside of 4 R_J (Region IV), we assume that the thermosphere and magnetosphere are perfectly coupled, with no load in the magnetosphere, such that $\Omega_M = \Omega_T$.

2.3. Coupling the Atmospheric and Magnetospheric Modules

We couple the 2.5-D thermospheric GCM and 1-D magnetosphere following the method described by SA09 and Y12. The thermospheric model is run continually over the prescribed runtime (Table 1). Every tenth of a planetary rotation, the height-averaged thermospheric velocity, from equations (1) and (2), is passed into the magnetospheric module. The magnetospheric module calculates the magnetospheric plasma angular velocity, electric fields, currents, field-aligned potentials, and ionospheric Pedersen conductance. Of these, the ionospheric Pedersen conductance and meridional electric field profiles are passed back to the thermospheric module and used to calculate the Joule heating and ion drag, both of which affect the thermospheric winds. To increase the stability of the numerical solver, the magnetospheric contribution is gradually raised to its full value over the first 20 rotations. The calculation continues until the model reaches steady-state. SA09 found that steady-state was reached after 200 Jovian rotations. Y12 determined that the relative difference in thermospheric height, temperature, and azimuthal velocity profiles between runs of 200 and 50 rotations was ~0.4%, ~0.8%, and ~1.2%, respectively, such that 50 rotations were sufficient to obtain a good approximation to the steady-state. For the purpose of this study, we run the model for 200 rotations, 100 rotations, and 50 rotations when comparing to SA09, R10, and Y12, respectively.

3. Results

To understand the relative effects of the mechanisms that affect angular momentum transport, i.e., variable Pedersen conductance, thermospheric feedback, and rotational decoupling allowed by high-latitude field-aligned potentials on M-I-T coupling, we compare results to three previous works: *Smith and Aylward* [2009], *Ray et al.* [2010], and *Yates et al.* [2012], which each couple two out of three of the listed mechanisms. For all runs, we assume a radial mass transport rate of 1000 kg s^{-1}. We place the high-latitude acceleration region at a mirror ratio of $R_x = 16$ following the work of *Ray et al.* [2010]. The high-latitude plasma population, which contributes to the electron thermal current, can be described with $n_x = 0.01$ cm^{-3}, $T_x = 2.5$ keV consistent with Voyager measurements of the hot plasma population at 17 R_J in the plasma sheet [*Scudder et al.*, 1981]. Table 1 lists the run parameters for each pair of comparisons.

3.1. Comparison With *Smith and Aylward* [2009]

SA09 were the first to numerically couple a thermospheric model to a dynamical model of plasma rotation in the magnetosphere. For a complete description of their model, the reader is referred to their original work. However, the main assumptions of their model are the following: (1) magnetic field lines are equipotentials; (2) the Pedersen conductance varies with field-aligned current density, following the description of *Nichols and Cowley* [2004]; (3) the outer magnetodisc boundary is located at 100 R_J; (4) the radial current at the

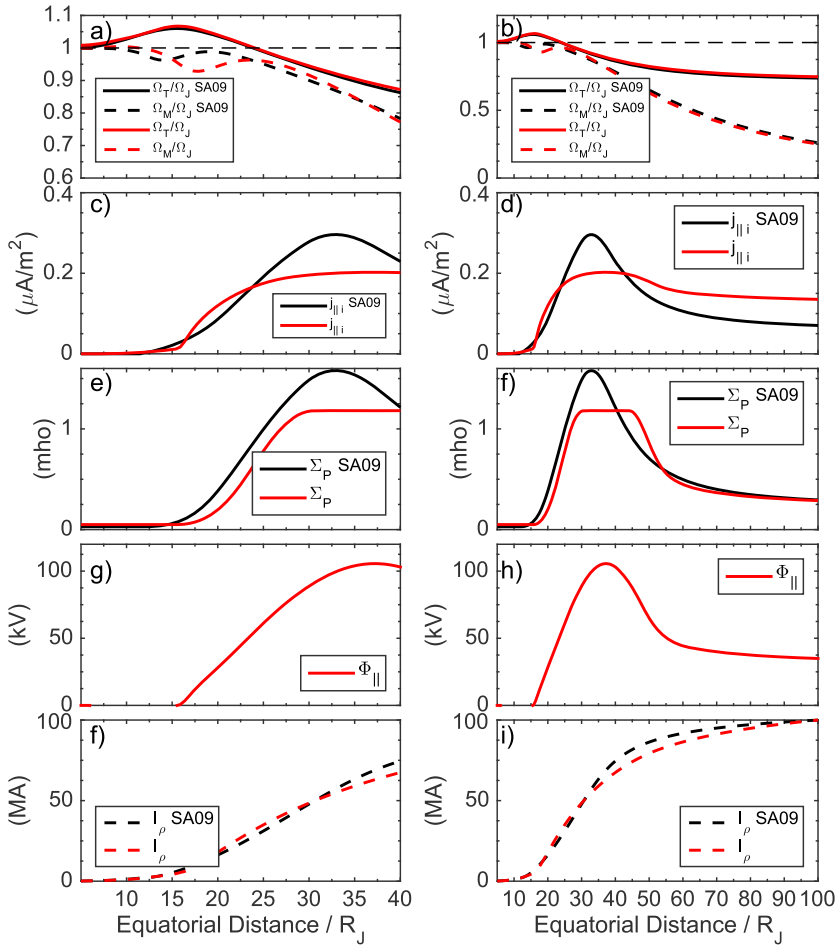

Figure 3. Profiles of the angular velocities, fields, and currents (a, c, e, g, and f) from 5 to 40 R_J and (b, d, f, h, and i) from 5 to 100 R_J . From top to bottom, the rows show the thermospheric and magnetospheric angular velocities, solid and dashed lines, respectively, ionospheric field-aligned current density, ionospheric Pedersen conductance, high-latitude field-aligned potentials, and magnetospheric radial current as a function of magnetospheric equatorial radius for the *Smith and Aylward* [2009] (black) and current (red) analyses. Note that parameters evaluated at the ionosphere, and then mapped to their magnetically conjugate location in the magnetosphere, are displayed with solid lines, whereas parameters evaluated in the magnetosphere are shown with dashed lines.

magnetodisc boundary, I_{100}, where the subscript indicates the location of the outer magnetodisc boundary, is 100 MA; and (5) thermospheric feedback is considered using the GCM.

Figure 3 displays profiles of the thermospheric and magnetospheric angular velocities (a and b), ionospheric field-aligned current densities (c), ionospheric Pedersen conductance (d), field-aligned potential strength (e), and radial current (f) from SA09 (black) and this analysis (red). The thermospheric angular velocity is similar between the two studies; however, there are significant differences in the magnetospheric angular velocities.

Inside of ~15 R_J, the differences in the magnetospheric angular velocity profiles are caused by the initial background Pedersen conductance. In the SA09 study $\Sigma_P^{\text{initial}}$=0.0275 mho, while in this study we use 0.05 mho so that the enhanced values of conductance from the two studies are comparable; however, Σ_P is not significantly enhanced until distances of ~15 R_J. Therefore, in the inner region, the magnetospheric plasma remains closer to corotation in the present study due to the larger ionospheric conductance, and hence increased angular momentum transfer between the planet and magnetosphere relative to the SA09 case.

Between ~15 R_J and ~24 R_J, predicted angular velocities from the SA09 study are closer to corotation. This difference is due to the variations in the **J** × **B** force exerted on the magnetospheric plasma. The shape of the field-aligned current density profile varies between the two models due to the differences in the nature of the

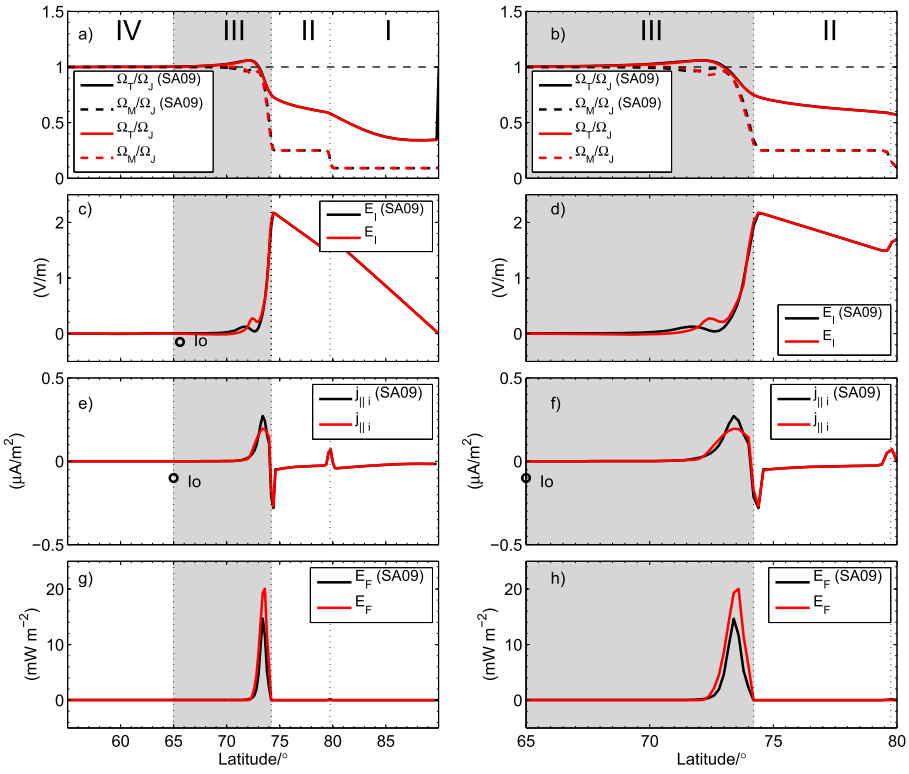

Figure 4. Latitudinal profiles of the (a and b) thermospheric (solid lines) and magnetospheric (dashed lines) angular velocities, (c and d) ionospheric electric fields, (e and f) ionospheric field-aligned current densities, and (g and h) auroral energy fluxes for the *Smith and Aylward* [2009] (black) and current analysis (red). The right-hand plots zoom in on Regions II and III.

Pedersen conductance enhancement between the two studies and the presence of field-aligned potentials in the present study.

For the SA09 case, the profile shapes for $J_{||}$ and Σ_P case are similar since their Pedersen conductance varied solely with field-aligned current density [*Nichols and Cowley*, 2004]. The Pedersen conductance function used here [*Ray et al.*, 2010] is a function of both the electron energy flux and the precipitating electron energy. The flat top to the Pedersen conductance profile occurs where the magnitude of the field-aligned potentials exceeds 80 kV (Figure 3e) such that the precipitating electrons deposit their energy below the peak conducting layer in the ionosphere. Via Ohm's law, $K = \Sigma_P E$, where K is the height-integrated current density in the ionosphere and E is the electric field in the rest frame of the thermospheric neutrals. If the conductivity is held fixed then the current density will vary with the electric field. Additionally, the ionospheric field-aligned current density is related to the magnitude of the field-aligned potentials through the *Knight* [1973] current-voltage relation and for $e\Phi_{||}/kT_x \gg R_x$, the current density will saturate. Therefore, the difference in the field-aligned current density profile arises from the interplay between the field-aligned potentials and Σ_P. Both the field-aligned current density and the ionospheric Pedersen conductance in the present study have reduced maximum magnitudes when compared to SA09, as seen in Figures 3c and 3d. However, the quantitative difference between the two studies only amounts to ~0.1 μA m^{-2}, or a reduction in the maximum $J_{||}$ of 30% from SA09. The SA09 Pedersen conductance increases from its background value enhancing the field-aligned current density at lower latitude, relative to the present study. As such the magnetospheric plasma returns toward corotation at smaller equatorial radii in the SA09 work.

Latitudinal profiles of the ionospheric and magnetospheric angular velocities (a and b), ionospheric field-aligned current densities (c and d), and auroral energy fluxes (e and f) are shown in Figure 4, which includes the boundary and polar regions, as well as the lower latitudes that couple to magnetospheric locations inside of Io's orbit. Following the magnetospheric angular velocity profiles, the magnitude of the ionospheric electric field is larger between 72° and 73.5° in the present study than in the SA09 work. The field-aligned current density at the ionosphere is qualitatively similar in both cases, with slight differences

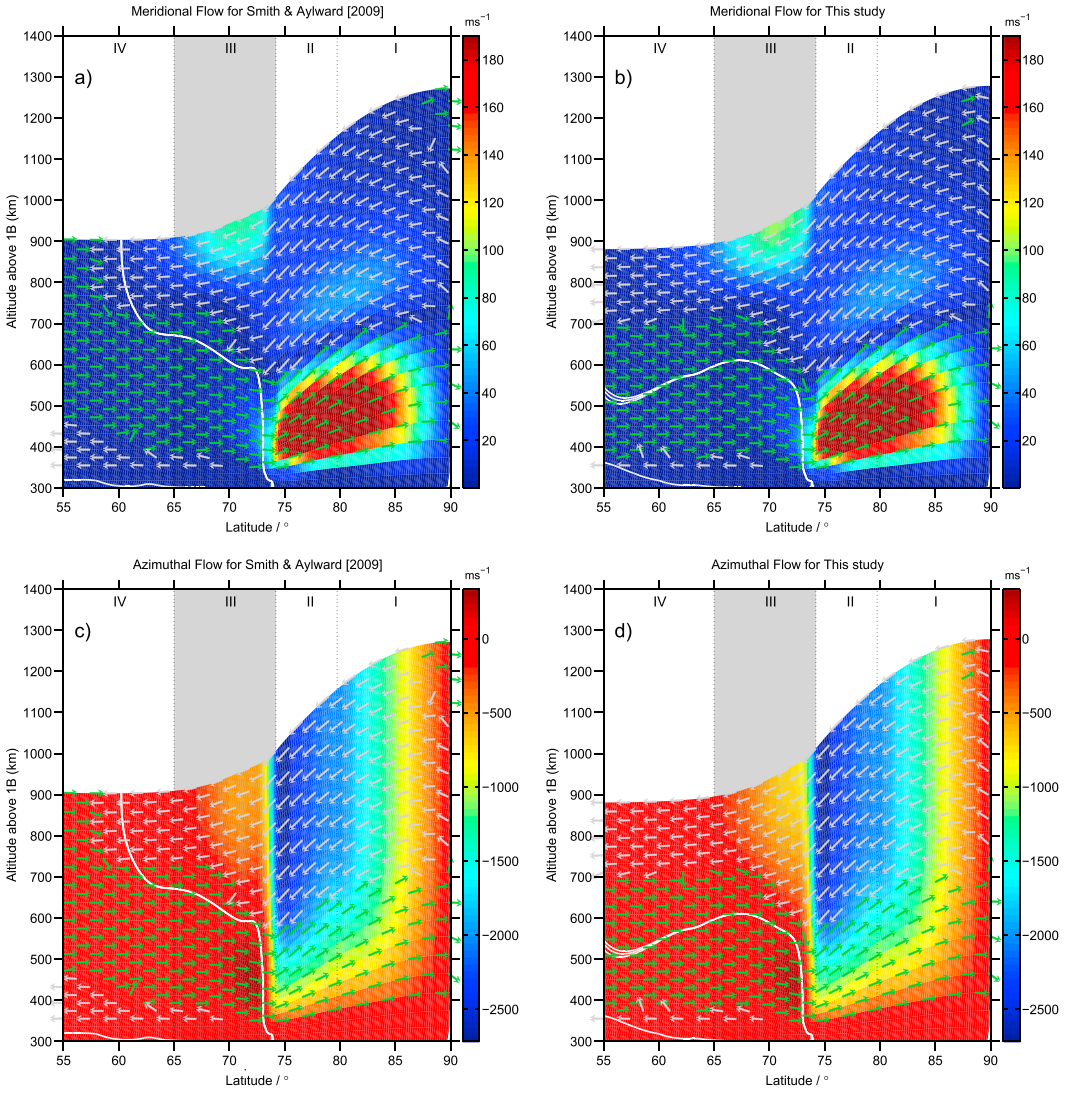

Figure 5. (a and b) Meridional and (c and d) azimuthal flows in the corotating reference frame for the *Smith and Aylward* [2009] (Figures 5a and 5c) and present (Figures 5b and 5d) study. The gray and green arrows represent the direction of the meridional flows, either equatorward or poleward, respectively. Flow magnitudes are displayed with the color scale for the meridional winds. For the azimuthal flows, the color scale shows the flow velocity. The white lines indicate where the azimuthal flow is corotational (0 m s^{-1}). Multiple white lines indicate a corotational flow channel.

in the magnitudes. However, the auroral energy fluxes predicted in the presence of field-aligned potentials, ~20 mW m^{-2}, are larger than the 14 mW m^{-2} derived from the *Smith and Aylward* [2009] study (note that the auroral energy fluxes were not calculated in the original study but are done so here following the methodology of *Nichols and Cowley*, 2004). Additionally, the modeled auroral oval is slightly broader in the present model by ~0.5° in latitude. In Regions I and II, the two models produce qualitatively similar results.

Figure 5 displays the thermospheric meridional (top) and azimuthal flows (bottom panels) for both the SA09 (left panels) and the present studies (right panels). In all panels, the arrows represent the direction of the meridional flows, with gray arrows flowing equatorward and green arrows flowing poleward. The solid white line is the locus of corotation where the azimuthal velocity is that of the deep planetary interior. The magnitude of the meridional flow, which is derived from both vertical and latitudinal components, is provided by the color scale in the top panels. In the bottom panels, the color scale shows the magnitude of the azimuthal flows with respect to corotation; hence, positive velocities indicate supercorotation while negative velocities correspond to subcorotational flows. The vertical dashed lines separate Regions I–IV as described in section 2.

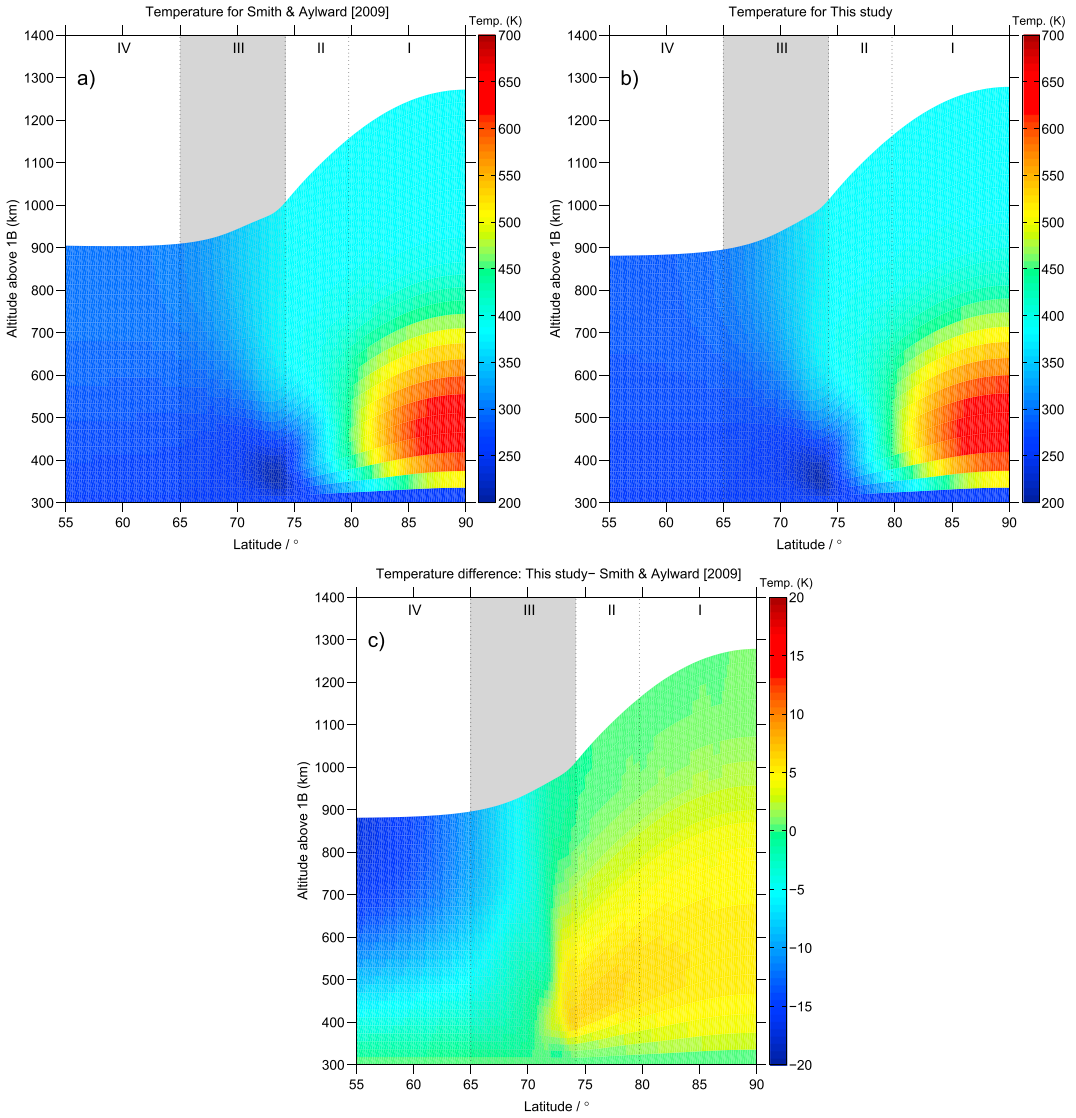

Figure 6. Thermospheric temperatures for the (a) *Smith and Aylward* [2009] study, (b) present study, and (c) temperature difference between the two models.

Perhaps the most obvious difference between the two simulated atmospheres is that at low latitudes and high altitudes, the meridional flow is directed equatorward in the current study, rather than poleward as in SA09. The increased meridional flows are due to the very slightly larger pressure gradient in the present study, relative to the SA09 work. It is important to note that the magnitude of these meridional flows is less than 5 m s^{-1}. In the azimuthal direction, the presence of field-aligned potentials increases the magnitude of the ionospheric electric field in Region III, driving a higher degree of subcorotation at high altitudes.

Figure 6 shows thermospheric temperature for the equipotential case (a), the temperature distribution for this study (b), and the difference between the two (c). The temperature difference is constructed using the common pressure grid of the two models and plotted against the corresponding altitude grid for this study. While a given pressure corresponds to different altitudes between the two studies, the maximum difference is 40 km, such that a qualitative comparison still valid. As seen clearly in Figure 6c, slightly more energy from Joule heating is transported to the polar regions in the present study. Thus, the "ion drag fridge" effect which prevents the transport of energy to low latitudes is still in operation when field-aligned potentials are included in the physical description of the system. Indeed, the effect is marginally enhanced from the SA09 work due to the increased meridional extent of the $\mathbf{J} \times \mathbf{B}$ force in the ionosphere. Figure 7 shows the momentum balance

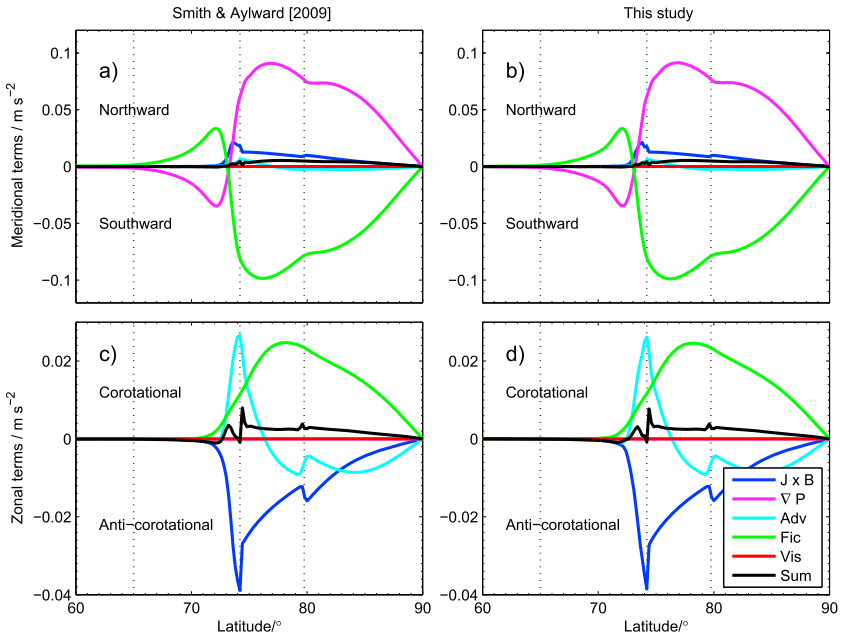

Figure 7. (a and b) Meridional and (c and d) zonal momentum terms for the *Smith and Aylward* [2009] (Figures 7a and 7c) and present study (Figures 7b and 7d). The fictitious force is the sum of the centrifugal and Coriolis forces.

of the thermosphere for both models. The meridional and zonal terms are nearly identical between the two studies, with the Coriolis forces balancing the pressure gradient terms in the meridional direction.

3.2. Comparison With *Ray et al.* [2010]

The magnetospheric calculation described in detail by R10 is the same one used in the current analysis. The relevant assumptions and parameters in their original work are the following: (1) field-aligned potentials are included in the electric field mapping through Faraday's law in the steady-state ($\nabla \times E = 0$), (2) Σ_P varies with both the electron energy flux and the electron precipitation energy, (3) the outer magnetodisc boundary is located at 100 R_J, (4) $I_{100} = 86$ MA, and (5) the thermosphere is treated simply, assuming $\Omega_T = \Omega_J$.

Figure 8 compares the thermospheric and magnetospheric angular velocities (a and b), ionospheric and magnetospheric electric fields (c and d), field-aligned current density (e), field-aligned potential (f), Pedersen conductance (g), and auroral energy flux (h) for this analysis (red lines) and the R10 analysis (black lines). The red lines in the Figures 8c and 8d show the electric field in the thermospheric reference frame for the current study, while the black and blue lines provide the field in the corotating reference frame. Note that the magnitude of the magnetospheric electric field is scaled to that of the ionosphere for ease of comparison. Qualitatively, the two systems behave similarly. In the present study, the thermosphere supercorotates between latitudes conjugate with ~6 and 17 R_J, lagging corotation outside ~17 R_J. The magnetospheric angular velocity slightly supercorotates from ~6 to 14 R_J, responding to the thermospheric supercorotation. Outside of 14 R_J, the magnetospheric plasma lags corotation, monotonically decreasing in its rotation rate.

For the remainder of the profiles, we will only discuss the behavior outside of ~15 R_J. The perpendicular electric field profiles are determined by the velocity lag of the plasma with respect to a chosen reference frame. In the R10 study, which neglected the subcorotation of the thermosphere, the relevant reference frame was that of corotation. When thermospheric effects are included, the appropriate reference frame for the determination of ionospheric electric fields and currents is that of the thermospheric neutrals. The current density is then frame independent. Comparing the R10 electric fields and the electric fields with those in the thermospheric neutral reference frame from the present study, the profiles are qualitatively similar. The ionospheric and magnetospheric electric fields map directly along the equipotential field lines until ~15 R_J where the field-aligned current exceeds the thermal current density. Field-aligned potentials develop at high magnetic latitudes outside this distance, and the electric mapping between the two regions is no

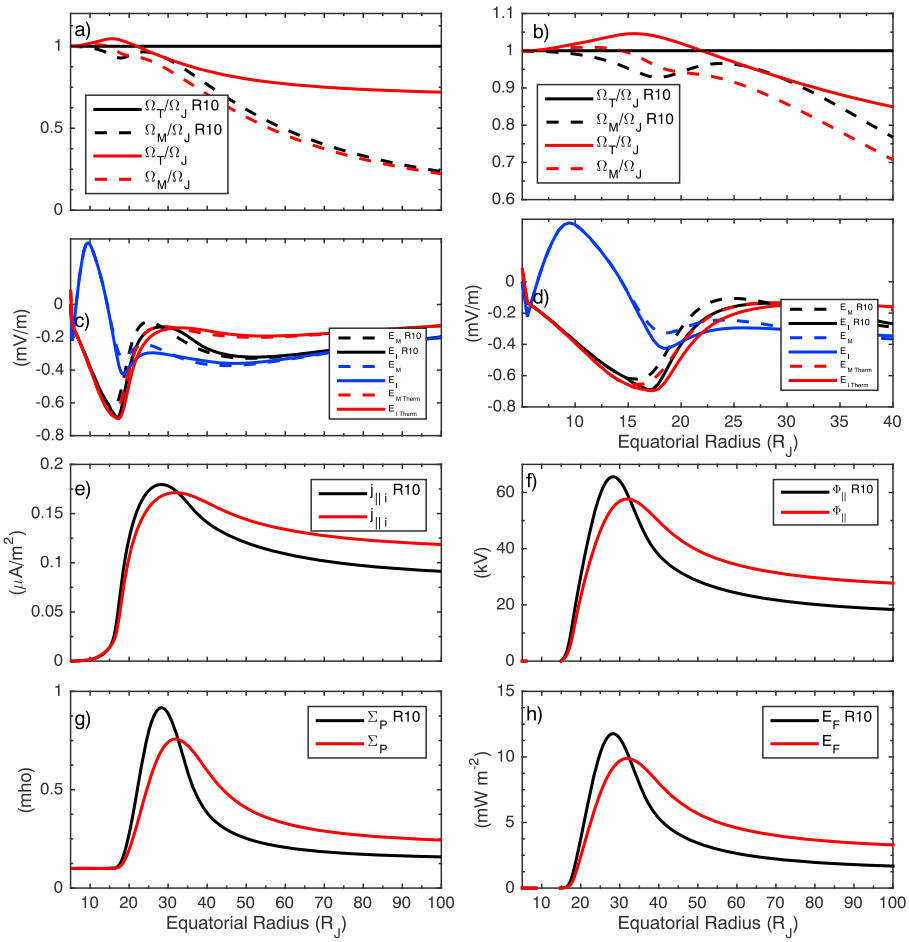

Figure 8. Profiles of the thermospheric and magnetospheric angular velocities (a) from 5 to 100 R_J and (b) from 5 to 40 R_J, ionospheric and magnetospheric perpendicular electric fields from (c) 5 to 100 R_J and (d) 5 to 40 R_J, (e) ionospheric field-aligned current density, (f) high-latitude field-aligned potentials, (g) ionospheric Pedersen conductance, and (h) auroral energy flux as a function of magnetospheric equatorial radius for the *Ray et al.* [2010] (black) and current (red) analyses. Note that parameters evaluated at the ionosphere, and then mapped to their magnetically conjugate location in the magnetosphere, are displayed with solid lines, whereas parameters evaluated in the magnetosphere are shown with dashed lines. In Figures 8c and 8d, the red lines show the electric fields in the frame corotating with the thermosphere; the blue and black lines give the electric field magnitudes in the corotating frame.

longer one-to-one, i.e., the mapping now also depends on the behavior of $\Phi_{||}$. Outside ~30 R_J the absolute magnitude of the ionospheric electric field in the present study is less than that in R10 due to the subcorotation of the thermosphere.

The field-aligned current density, field-aligned potential, Pedersen conductance, and energy flux profiles all show similar trends, where the values predicted by the R10 model exceed those from the present study inside of 32 R_J. Outside this distance, the present analysis predicts larger values. When the thermospheric rotation rate is self-consistently calculated, the difference between the rotation rate of the thermosphere and magnetospheric plasma is smaller than in the case of corotation. In this case, smaller magnitude field-aligned currents transfer the angular momentum from the atmosphere to the magnetosphere, resulting in decreased field-aligned potentials and a reduced Pedersen conductance.

Beyond ~32 R_J, the location where the $\mathbf{J} \times \mathbf{B}$ force is no longer sufficient to accelerate the plasma toward corotation, the deviation of the magnetospheric angular velocity again increases, and with it the magnitude of magnetospheric electric field. The field-aligned potential profile turns over and decreases. The relative variation in the ionospheric and magnetospheric electric fields with latitude decreases, such that the radial

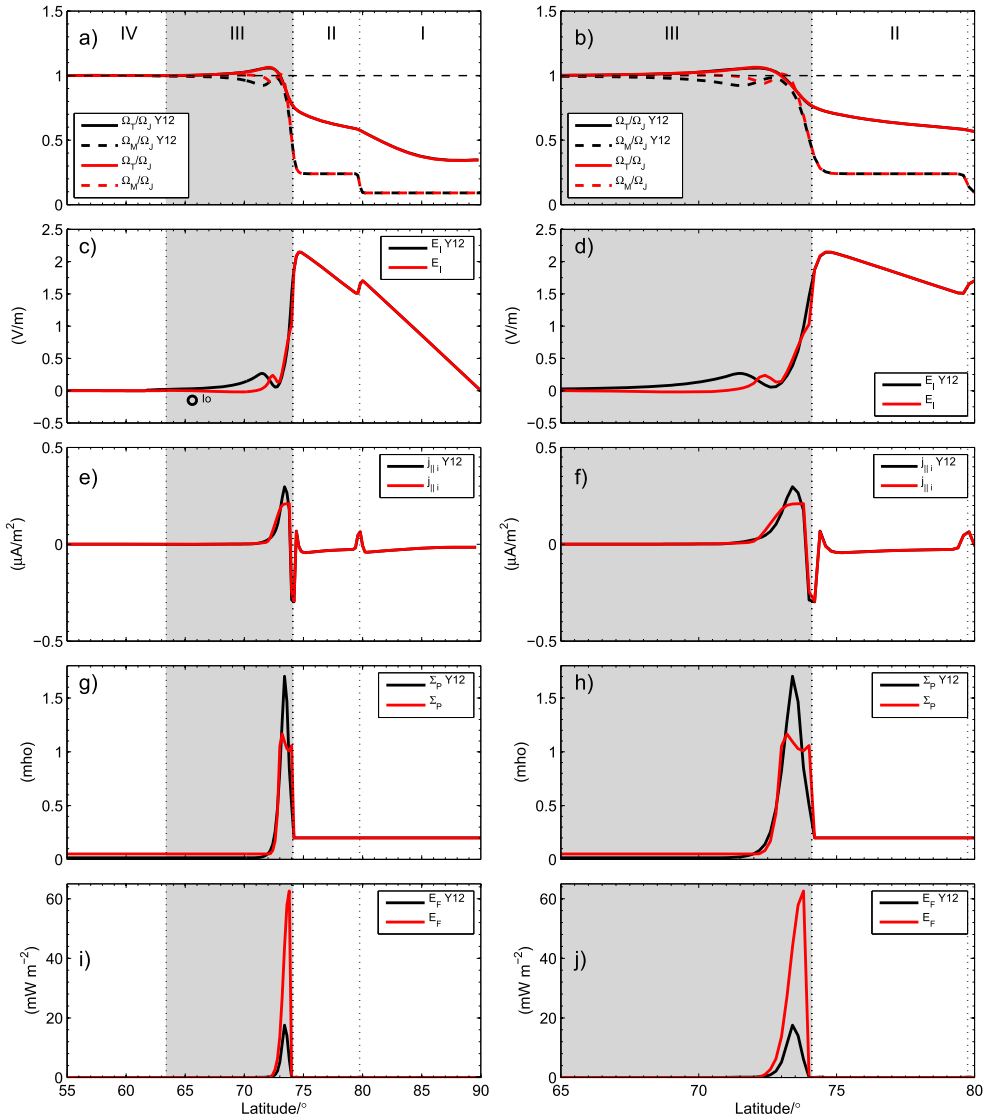

Figure 9. Latitudinal profiles of the (a and b) thermospheric (solid lines) and magnetospheric (dashed lines) angular velocities, (c and d) ionospheric electric fields, (e and f) ionospheric field-aligned current densities, (g and h) Pedersen conductances, and (i and j) auroral energy fluxes for the *Yates et al.* [2012] (black) baseline case and current analysis (red). Figures 9a, 9c, 9e, 9g, and 9i show Regions I–IV, while Figures 9b, 9d, 9f, 9h, and 9j zoom in on Regions II and III.

gradient of the field-aligned potentials approaches zero and the magnetic field lines can be approximately described as equipotentials.

In the present study, the predicted auroral emission intensities are decreased by ~20% relative to the R10 work. This is directly related to the reduced magnitude of the field-aligned potentials and field-aligned current densities necessary to transport angular momentum, which are in turn due to the reduced angular velocity difference because of the more subcorotational thermosphere.

3.3. Comparison With *Yates et al.* [2012]

The Y12 model is identical to that of SA09 except that the outer edge of the magnetodisc can be placed at distances of 45 R_J, 65 R_J, and 85 R_J. We focus on the Y12 baseline case where the magnetodisc boundary is placed at 65 R_J and the radial current at the edge of the magnetodisc is 100 MA. Here we fix the location of the acceleration region at ~2.5 R_J along the field ($R_x = 16$).

Figure 9 displays the latitudinal profiles of the magnetospheric and thermospheric angular velocities (a and b), ionospheric electric field (c and d), ionospheric field-aligned current density (e and f), Pedersen conductance

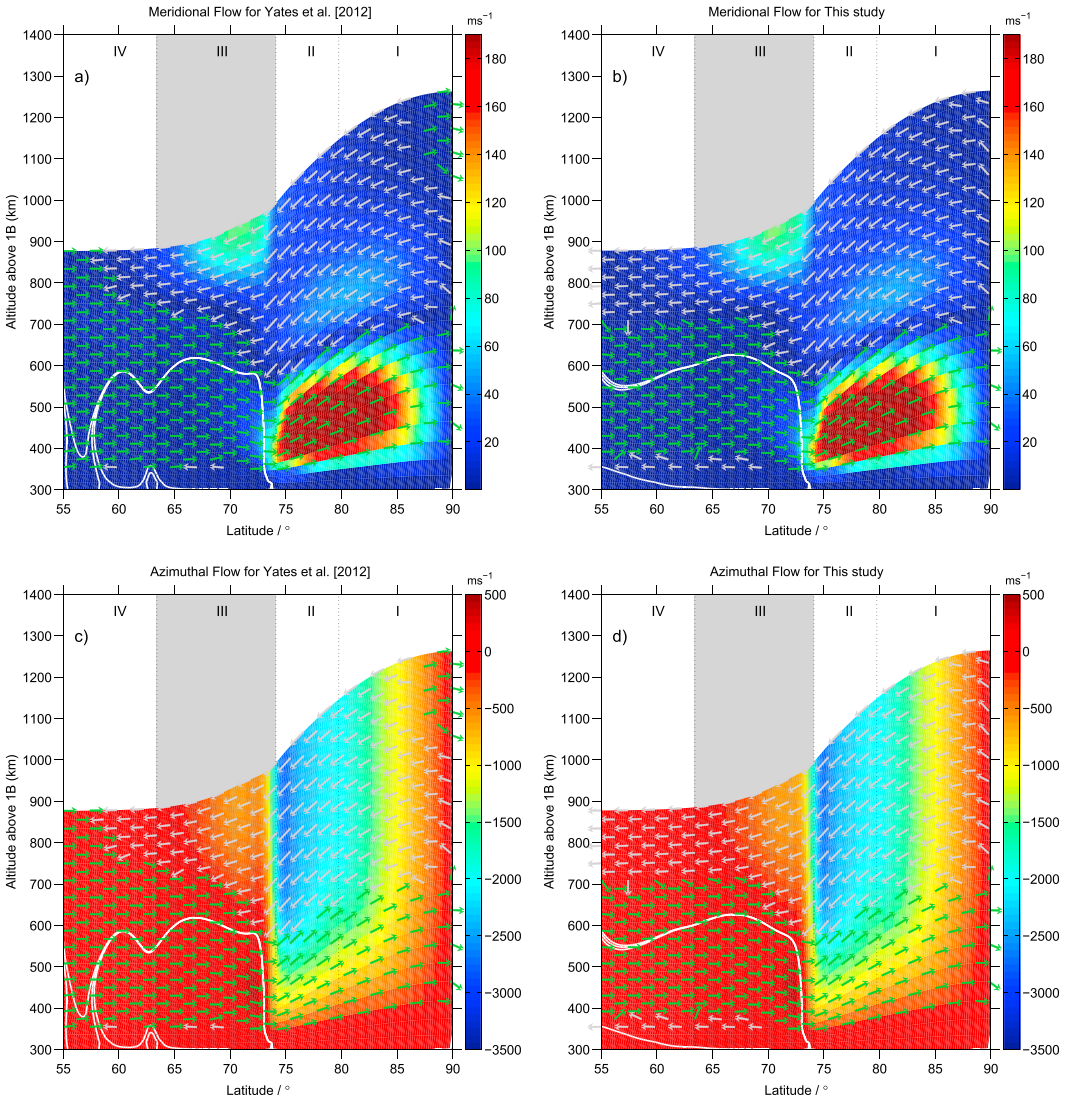

Figure 10. Same as Figure 5 but comparing the *Yates et al.* [2012] and present studies.

(g and h), and auroral energy fluxes (i and j). As in the SA09 case, the magnetospheric and thermospheric angular velocity profiles between the Y12 work and present study are similar. In the present study, the magnetospheric plasma remains near corotation to higher latitudes than in the Y12 case. Thus, the magnitude of the ionospheric electric field is smaller in the present study, decreasing the $\mathbf{J} \times \mathbf{B}$ force in the ionosphere. The maximum field-aligned current density is comparable between the two studies; however, because of the large magnitude of the outer current constraint, $I_{65} = 100$ MA, the ionospheric current density saturates over a narrow latitudinal range spanning 73°–74° in the present work. As outlined in R10, the interplay of the Pedersen conductance and ionospheric electric field break the current saturation. When the current density is saturated, the field-aligned potentials maximize at 230 kV. Hence, the predicted auroral energy fluxes are over 3 times greater than those predicted by Y12.

Thermospheric flows are displayed in Figure 10. Immediately, one notices that the flows are very similar between the two cases. Similar to the SA09 comparison, there is increased equatorward meridional flow at high altitudes and low latitudes. The poleward transport of energy and momentum remains relatively unchanged. As expected, the azimuthal flows are similar since the $\mathbf{J} \times \mathbf{B}$ varies only slightly between the two studies.

The temperature structure of the atmosphere is shown in Figure 11 for Y12 (a), the present study (b), and the difference between the two (c). Within ~3 K, the two studies produce the same temperature profiles.

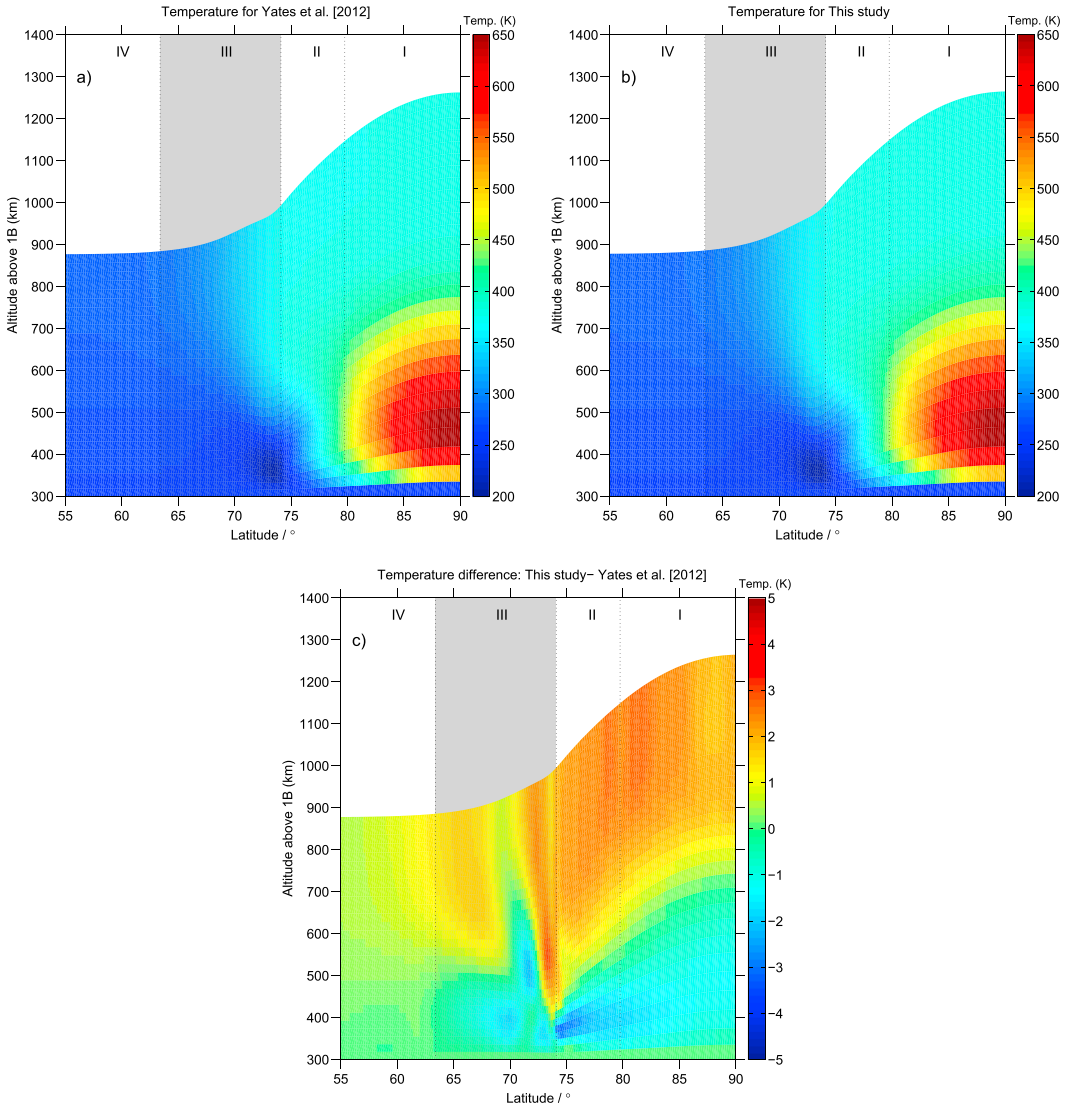

Figure 11. Same as Figure 6 but comparing the *Yates et al.* [2012] and present studies.

The temperature of the polar hot spot is slightly reduced from the Y12 study, with more energy reaching high altitudes. The fluctuations in the temperature, best seen in Figure 11c, are coincident with the dip in the Pedersen conductance in the location where the precipitating electron energies are greater than 80 keV, highlighting the control of the conductivity on the M-I-T coupled system.

Figure 12 provides the momentum balance between the meridional (a and b) and zonal (c and d) terms of Y12 (a and c) and the present study (b and d). The most noticeable difference is in the shape of the meridional $\mathbf{J} \times \mathbf{B}$ term between 73° and 75° latitude. In the present study, the $\mathbf{J} \times \mathbf{B}$ term is more sustained between 73° and 75° latitude, rather than peaking at ~74° and then decreasing. Correspondingly, the fictitious force (Coriolis + centrifugal) and advective terms are slightly modified from the Y12 case.

4. Discussion

We have considered the effect of rotational decoupling between the ionosphere and magnetosphere in a coupled thermosphere-ionosphere-magnetosphere model. The resulting model has been compared to three previous studies, two of which explicitly considered the effect of the thermosphere on the magnetosphere, but assumed perfect coupling between the ionosphere and magnetosphere (i.e., ignored the influence of field-aligned potentials), and one that treated the thermosphere simply, but included rotational decoupling between the ionosphere and the magnetosphere.

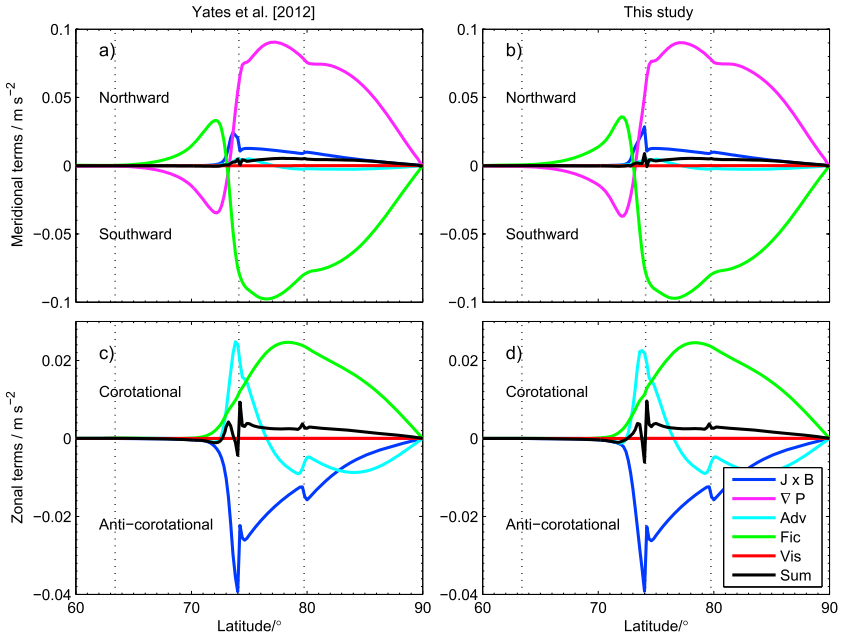

Figure 12. Same as Figure 7 but comparing the *Yates et al.* [2012] and present studies.

Surprisingly, the magnetospheric angular velocities of this study compare most easily to the SA09 analysis, which included thermospheric effects and a variable Pedersen conductance but neglected the rotational decoupling due to field-aligned potentials. This indicates that the thermosphere and conductance play more dominant roles in keeping the magnetospheric plasma corotational than do field-aligned potentials. However, the opposite trend applies when predicting the current densities, Pedersen conductances, and intensity of the auroral emission. This is to be expected due to the different methods of determining the auroral intensity. In the present work, and the R10 study, the auroral energy flux is provided as $J_{||}\Phi_{||}$ where $J_{||}$ and $\Phi_{||}$ are related through the *Knight* [1973] relationship applied at high latitudes. The Y12 study determined the auroral energy flux through use of the linear approximation to the Knight relations [*Lyons*, 1980]. Under the conditions of the Y12 analysis, i.e., a magnetodisc size of 65 R_J with 100 MA of radial current at the outer boundary, this difference amounts to the present study predicting an auroral intensity 3 times brighter than the original work. *Gustin et al.* [2004] found that the typical main auroral intensity ranges from 2 to 30 mW m^{-2}, thus the maximum intensity predicted here, 60 mW m^{-2}, corresponds to a value more typical for storm conditions [*Gustin et al.*, 2006].

The Pedersen conductance formulation used in this analysis varies from that of SA09 and Y12. This may cause some of the variations detailed in section 3. However, this highlights the importance of the Pedersen conductance in the driving of the system dynamics. Small variations in the feedback between the current system transporting angular momentum and the modification of the Pedersen conductance can drive different dynamics in both the atmosphere and the magnetosphere. At the moment, Jupiter's Pedersen conductance is poorly constrained. There have been estimates based on radio occultation data from the Pioneer 10 and 11 flybys, yet these profiles were not taken at high latitudes. Measurements of the ionospheric electron density at high latitudes would greatly improve our understanding of the system. [*Millward et al.*, 2002] determined the conductivity profile as a function of either precipitating electron energy flux or number flux using a 3-D model of the Jovian ionosphere and thermosphere. However, their study used a monoenergetic beam of electrons precipitating into the atmosphere directly along the vertical. Improved modeling of the Pedersen conductivity profile with auroral energy inputs would allow better parameterization of conductance as a function of energy flux and particle energy.

In terms of atmospheric effects, field-aligned potentials do not significantly modify the thermospheric energy distribution and flows. At high altitudes and midlatitudes, the increased equatorward transport is marginal as the flow magnitude in that region is less than 5 m s^{-1}. The temperature profiles are similar in the SA09 and Y12

comparisons within 10 K and 3 K, respectively. In the SA09 comparison, more energy is transported poleward whereas in the Y12 comparison slightly less energy is transported poleward.

In Regions I and II, the behavior at high latitudes is dictated by the Pedersen conductance and the imposed flows. If the Pedersen conductance in the polar cap is different from the 0.2 mho assumed here, the thermospheric flows will be altered. Indeed, if the Pedersen conductance is decreased, preliminary studies indicate that more auroral energy is transported equatorward.

In reality, the Jovian system is neither steady-state nor axisymmetric. However, within the axisymmetric framework, recent work by *Yates et al.* [2014] has shown that rapid (~3 h) magnetospheric compressions and expansions can trigger equatorward heat transport. These events directly affect the size of the magnetodisc and the plasma angular velocity profile, which in turn modify the auroral currents and ionospheric electric field. To date, no model of the nature we have described herein has explored a nonaxisymmetric magnetodisc. Outside of 20 R_J, the assumption of axisymmetry begins to falter in Jupiter's magnetosphere. *Vogt et al.* [2011] used Galileo data to show that the normal component of the magnetic field in the center of the current sheet has strong variations in local time. *Ray et al.* [2014] showed that these variations affect the $\mathbf{J} \times \mathbf{B}$ force exerted on the plasma, thereby modifying the auroral currents as a function of local time. Indeed, UV auroral observations show a narrower band of auroral emission on the dawnside of the planet and broader, diffuse emission on the duskside. *Radioti et al.* [2008] found a persistent discontinuity in the main emission near noon, which may correspond to the downward current region suggested by Galileo data [*Khurana*, 2001]. Investigating such local time variations in the magnetic field structure, and hence auroral currents and thermospheric flows, is a logical next step in this work.

In summary, a treatment of the thermosphere-ionosphere-magnetosphere system, which self-consistently includes field-aligned potentials at high magnetic latitudes, offers new insight into Jupiter's auroral currents and thermospheric properties. The main results are

1. Inclusion of field-aligned potentials does not significantly affect the thermospheric dynamics and energy distribution when compared to previous models.
2. Variations in the Pedersen conductance have the strongest effect on system dynamics.
3. For the case with a magnetodisc size of 65 R_J, the present model predicts auroral intensities larger than those inferred from observations of the typical auroral emission.

Acknowledgments

L.C.R. was supported by NSF grant 1064635 and by STFC's UCL Astrophysics Consolidated grant ST/J001511/1. L.C.R. would also like to acknowledge the ISSI teams on Comparative Jovian Aeronomy for useful discussions. N.A. was supported by STFC's UCL Astrophysics Consolidated grant ST/J001511/1. J.N.Y. was supported by STFC's Imperial College Astrophysics and Space Physics Consolidated grant ST/K001051/1. The authors acknowledge support of computational resources provided as part of the STFC-funded Miracle project (now completed) and support from the ISSI team on Coordinated Numerical Modelling of the Global Jovian and Saturnian Systems. The authors would also like to thank Chris Smith for making his data available and useful conversations, and the referees for useful comments. The model runs presented here are available upon request from L.C.R.

Larry Kepko thanks two anonymous reviewers for their assistance in evaluating this paper.

References

Achilleos, N., S. Miller, J. Tennyson, A. D. Aylward, I. Mueller-Wodarg, and D. Rees (1998), JIM: A time-dependent, three-dimensional model of Jupiter's thermosphere and ionosphere, *J. Geophys. Res.*, *103*, 20,089–20,112, doi:10.1029/98JE00947.

Bonfond, B., D. Grodent, J.-C. Gérard, T. Stallard, J. T. Clarke, M. Yoneda, A. Radioti, and J. Gustin (2012), Auroral evidence of Io's control over the magnetosphere of Jupiter, *Geophys. Res. Lett.*, *39*, L01105, doi:10.1029/2011GL050253.

Branduardi-Raymont, G., R. F. Elsner, M. Galand, D. Grodent, T. E. Cravens, P. Ford, G. R. Gladstone, and J. H. Waite (2008), Spectral morphology of the X-ray emission from Jupiter's aurorae, *J. Geophys. Res.*, *113*, A02202, doi:10.1029/2007JA012600.

Clarke, J. T., L. Ben Jaffel, and J.-C. Gérard (1998), Hubble Space Telescope imaging of Jupiter's UV aurora during the Galileo orbiter mission, *J. Geophys. Res.*, *103*, 20,217–20,236, doi:10.1029/98JE01130.

Clarke, J. T., D. Grodent, S. W. H. Cowley, E. J. Bunce, P. Zarka, J. E. P. Connerney, and T. Satoh (2004), Jupiter's aurora, in *Jupiter. The Planet, Satellites and Magnetosphere, Cambridge Planet. Sci.*, edited by F. Bagenal, T. E. Dowling, and W. B. McKinnon, pp. 639–670, Cambridge Univ. Press, Cambridge, U. K.

Cowley, S. W. H., I. I. Alexeev, E. S. Belenkaya, E. J. Bunce, C. E. Cottis, V. V. Kalegaev, J. D. Nichols, R. Prangé, and F. J. Wilson (2005), A simple axisymmetric model of magnetosphere-ionosphere coupling currents in Jupiter's polar ionosphere, *J. Geophys. Res.*, *110*, A11209, doi:10.1029/2005JA011237.

Delamere, P. A., and F. Bagenal (2003), Modeling variability of plasma conditions in the Io torus, *J. Geophys. Res.*, *108*(A7), 1276, doi:10.1029/2002JA009706.

Delamere, P. A., A. Steffl, and F. Bagenal (2004), Modeling temporal variability of plasma conditions in the Io torus during the Cassini era, *J. Geophys. Res.*, *109*, A10216, doi:10.1029/2003JA010354.

Delamere, P. A., F. Bagenal, and A. Steffl (2005), Radial variations in the Io plasma torus during the Cassini era, *J. Geophys. Res.*, *110*, A12223, doi:10.1029/2005JA011251.

Gérard, J.-C., D. Grodent, A. Radioti, B. Bonfond, and J. T. Clarke (2013), Hubble observations of Jupiter's north-south conjugate ultraviolet aurora, *Icarus*, *226*, 1559–1567, doi:10.1016/j.icarus.2013.08.017.

Grodent, D., J. H. Waite Jr., and J.-C. Gérard (2001), A self-consistent model of the Jovian auroral thermal structure, *J. Geophys. Res.*, *106*, 12,933–12,952, doi:10.1029/2000JA900129.

Grodent, D., J. T. Clarke, J. Kim, J. H. Waite, and S. W. H. Cowley (2003), Jupiter's main auroral oval observed with HST-STIS, *J. Geophys. Res.*, *108*(A11), 1389, doi:10.1029/2003JA009921.

Grodent, D., J. Gérard, A. Radioti, B. Bonfond, and A. Saglam (2008), Jupiter's changing auroral location, *J. Geophys. Res.*, *113*, A01206, doi:10.1029/2007JA012601.

Gustin, J., J.-C. Gérard, D. Grodent, S. W. H. Cowley, J. T. Clarke, and A. Grard (2004), Energy-flux relationship in the FUV Jovian aurora deduced from HST-STIS spectral observations, *J. Geophys. Res.*, *109*, A10205, doi:10.1029/2003JA010365.

Gustin, J., S. W. H. Cowley, J.-C. Gérard, G. R. Gladstone, D. Grodent, and J. T. Clarke (2006), Characteristics of Jovian morning bright FUV aurora from Hubble Space Telescope/Space Telescope Imaging Spectrograph imaging and spectral observations, *J. Geophys. Res.*, *111*, A09220, doi:10.1029/2006JA011730.

Hickey, M. P., R. L. Walterscheid, and G. Schubert (2000), Gravity wave heating and cooling in Jupiter's thermosphere, *Icarus*, *148*, 266–281, doi:10.1006/icar.2000.6472.

Huang, T. S., and T. W. Hill (1989), Corotation lag of the Jovian atmosphere, ionosphere, and magnetosphere, *J. Geophys. Res.*, *94*, 3761–3765.

Isbell, J., A. J. Dessler, and J. H. Waite Jr. (1984), Magnetospheric energization by interaction between planetary spin and the solar wind, *J. Geophys. Res.*, *89*, 10,716–10,722, doi:10.1029/JA089iA12p10716.

Khurana, K. K. (2001), Influence of solar wind on Jupiter's magnetosphere deduced from currents in the equatorial plane, *J. Geophys. Res.*, *106*, 25,999–26,016, doi:10.1029/2000JA000352.

Knight, S. (1973), Parallel electric fields, *Planet. Space Sci.*, *21*, 741–750.

Lyons, L. R. (1980), Generation of large-scale regions of auroral currents, electric potentials, and precipitation by the divergence of the convection electric field, *J. Geophys. Res.*, *85*, 17–24.

Matcheva, K. I., and D. F. Strobel (1999), Heating of Jupiter's thermosphere by dissipation of gravity waves due to molecular viscosity and heat conduction, *Icarus*, *140*, 328–340, doi:10.1006/icar.1999.6151.

Melin, H., S. Miller, T. Stallard, C. Smith, and D. Grodent (2006), Estimated energy balance in the Jovian upper atmosphere during an auroral heating event, *Icarus*, *181*, 256–265, doi:10.1016/j.icarus.2005.11.004.

Millward, G., S. Miller, T. Stallard, A. D. Aylward, and N. Achilleos (2002), On the dynamics of the Jovian ionosphere and thermosphere: III. The modelling of auroral conductivity, *Icarus*, *160*, 95–107, doi:10.1006/icar.2002.6951.

Millward, G., S. Miller, T. Stallard, N. Achilleos, and A. D. Aylward (2005), On the dynamics of the Jovian ionosphere and thermosphere: IV. Ion-neutral coupling, *Icarus*, *173*, 200–211, doi:10.1016/j.icarus.2004.07.027.

Nichols, J. D. (2011), Magnetosphere-ionosphere coupling currents in Jupiter's middle magnetosphere: Computations including a self-consistent current sheet magnetic field model, *J. Geophys. Res.*, *116*, A10232, doi:10.1029/2011JA016922.

Nichols, J. D., and S. W. H. Cowley (2004), Magnetosphere-ionosphere coupling currents in Jupiter's middle magnetosphere: Effect of precipitation-induced enhancement of the ionospheric Pedersen conductivity, *Ann. Geophys.*, *22*, 1799–1827, doi:10.5194/angeo-22-1799-2004.

Nichols, J. D., J. T. Clarke, J. C. Gérard, D. Grodent, and K. C. Hansen (2009), Variation of different components of Jupiter's auroral emission, *J. Geophys. Res.*, *114*, A06210, doi:10.1029/2009JA014051.

Pontius, D. H. (1995), Implications of variable mass loading in the Io torus: The Jovian flywheel, *J. Geophys. Res.*, *100*, 19,531–19,540, doi:10.1029/95JA01554.

Radioti, A., J. Gérard, D. Grodent, B. Bonfond, N. Krupp, and J. Woch (2008), Discontinuity in Jupiter's main auroral oval, *J. Geophys. Res.*, *113*, A01215, doi:10.1029/2007JA012610.

Ray, L. C., Y. Su, R. E. Ergun, P. A. Delamere, and F. Bagenal (2009), Current-voltage relation of a centrifugally confined plasma, *J. Geophys. Res.*, *114*, A04214, doi:10.1029/2008JA013969.

Ray, L. C., R. E. Ergun, P. A. Delamere, and F. Bagenal (2010), Magnetosphere-ionosphere coupling at Jupiter: Effect of field-aligned potentials on angular momentum transport, *J. Geophys. Res.*, *115*, A09211, doi:10.1029/2010JA015423.

Ray, L. C., N. A. Achilleos, M. F. Vogt, and J. N. Yates (2014), Local time variations in Jupiter's magnetosphere-ionosphere coupling system, *J. Geophys. Res. Space Physics*, *119*, 4740–4751, doi:10.1002/2014JA019941.

Schubert, G., M. P. Hickey, and R. L. Walterscheid (2003), Heating of Jupiter's thermosphere by the dissipation of upward propagating acoustic waves, *Icarus*, *163*, 398–413, doi:10.1016/S0019-1035(03)00078-2.

Scudder, J. D., E. C. Sittler, and H. S. Bridge (1981), A survey of the plasma electron environment of Jupiter—A view from Voyager, *J. Geophys. Res.*, *86*, 8157–8179.

Seiff, A., D. B. Kirk, T. C. D. Knight, R. E. Young, J. D. Mihalov, L. A. Young, F. S. Milos, G. Schubert, R. C. Blanchard, and D. Atkinson (1998), Thermal structure of Jupiter's atmosphere near the edge of a 5-μm hot spot in the north equatorial belt, *J. Geophys. Res.*, *103*, 22,857–22,890, doi:10.1029/98JE01766.

Smith, C. G. A., and A. D. Aylward (2008), Coupled rotational dynamics of Saturn's thermosphere and magnetosphere: A thermospheric modelling study, *Ann. Geophys.*, *26*, 1007–1027, doi:10.5194/angeo-26-1007-2008.

Smith, C. G. A., and A. D. Aylward (2009), Coupled rotational dynamics of Jupiter's thermosphere and magnetosphere, *Ann. Geophys.*, *27*, 199–230.

Smith, C. G. A., S. Miller, and A. D. Aylward (2005), Magnetospheric energy inputs into the upper atmospheres of the giant planets, *Ann. Geophys.*, *23*, 1943–1947, doi:10.5194/angeo-23-1943-2005.

Stallard, T., S. Miller, G. Millward, and R. D. Joseph (2001), On the dynamics of the Jovian ionosphere and thermosphere: I. The measurement of ion winds, *Icarus*, *154*, 475–491, doi:10.1006/icar.2001.6681.

Stallard, T., S. Miller, G. Millward, and R. D. Joseph (2002), On the dynamics of the Jovian ionosphere and thermosphere: II. The measurement of H_3^+ vibrational temperature, column density, and total emission, *Icarus*, *156*, 498–514, doi:10.1006/icar.2001.6793.

Strobel, D. F., and G. R. Smith (1973), On the temperature of the Jovian thermosphere, *J. Atmos. Sci.*, *30*, 718–725, doi:10.1175/1520-0469(1973)030<0718:OTTOTJ>2.0.CO;2.

Su, Y., R. E. Ergun, F. Bagenal, and P. A. Delamere (2003), Io-related Jovian auroral arcs: Modeling parallel electric fields, *J. Geophys. Res.*, *108*(A6), 1094, doi:10.1029/2002JA009247.

Vasavada, A. R., A. H. Bouchez, A. P. Ingersoll, B. Little, C. D. Anger, and Galileo SSI Team (1999), Jupiter's visible aurora and Io footprint, *J. Geophys. Re.*, *104*, 27,133–27,142, doi:10.1029/1999JE001055.

Vogt, M. F., M. G. Kivelson, K. K. Khurana, R. J. Walker, B. Bonfond, D. Grodent, and A. Radioti (2011), Improved mapping of Jupiter's auroral features to magnetospheric sources, *J. Geophys. Res.*, *116*, A03220, doi:10.1029/2010JA016148.

Yates, J. N., N. Achilleos, and P. Guio (2012), Influence of upstream solar wind on thermospheric flows at Jupiter, *Planet. Space Sci.*, *61*, 15–31, doi:10.1016/j.pss.2011.08.007.

Yates, J. N., N. Achilleos, and P. Guio (2014), Response of the Jovian thermosphere to a transient pulse in solar wind pressure, *Planet. Space Sci.*, *91*, 27–44, doi:10.1016/j.pss.2013.11.009.

Young, L. A., R. V. Yelle, R. Young, A. Seiff, and D. B. Kirk (1997), Gravity waves in Jupiter's thermosphere, *Science*, *276*, 108–111, doi:10.1126/science.276.5309.108.